crystals

MDPI

Article

Structural Characterization of β-Xylosidase XynB2 from *Geobacillus stearothermophilus* CECT43: A Member of the Glycoside Hydrolase Family GH52

Jose Antonio Gavira [1], Lellys M. Contreras [2], Hassan Mohamad Alshamaa [1,3], Josefa María Clemente-Jiménez [2], Felipe Rodríguez-Vico [2], Francisco Javier Las Heras-Vázquez [2] and Sergio Martínez-Rodríguez [1,3,*]

[1] Laboratorio de Estudios Cristalográficos, Instituto Andaluz de Ciencias de la Tierra (IACT, CSIC), Universidad de Granada, 18100 Granada, Spain; jgavira@iact.ugr-csic.es (J.A.G.); hassan.alshamaa1@gmail.com (H.M.A.)
[2] Departamento de Química y Física, Universidad de Almería, 04120 Almería, Spain; mariela@ual.es (L.M.C.); jmclemen@ual.es (J.M.C.-J.); fvico@ual.es (F.R.-V.); fjheras@ual.es (F.J.L.H.-V.)
[3] Departamento de Bioquímica y Biología Molecular III e Inmunología, Universidad de Granada, 18100 Granada, Spain
* Correspondence: sergio@ugr.es

Abstract: β-xylosidases (4-β-D-xylan xylohydrolase, E.C. 3.2.1.37) are glycoside hydrolases (GH) catalyzing the hydrolysis of (1→4)-β-D-xylans, allowing for the removal of β-D-xylose residues from its non-reducing termini. Together with other xylan-degrading enzymes, β-xylosidases are involved in the enzymatic hydrolysis of lignocellulosic biomass, making them highly valuable in the biotechnological field. Whereas different GH families are deeply characterized from a structural point of view, the GH52 family has been barely described. In this work, we report the 2.25 Å resolution structure of *Geobacillus stearothermophilus* CECT43 XynB2, providing the second structural characterization for this GH family. A plausible dynamic loop closing the entrance of the catalytic cleft is proposed based on the comparison of the available GH52 structures, suggesting the relevance of a dimeric structure for members of this family. The glycone specificity at the −1 site for GH52 and GH116 members is also explained by our structural studies.

Keywords: crystallization of β-xylosidase; XynB2; Glycoside Hydrolase Family 52; Glycoside Hydrolase Family 116

Citation: Gavira, J.A.; Contreras, L.M.; Alshamaa, H.M.; Clemente-Jiménez, J.M.; Rodríguez-Vico, F.; Las Heras-Vázquez, F.J.; Martínez-Rodríguez, S. Structural Characterization of β-Xylosidase XynB2 from *Geobacillus stearothermophilus* CECT43: A Member of the Glycoside Hydrolase Family GH52. *Crystals* **2024**, *14*, 18. https://doi.org/10.3390/cryst14010018

Academic Editor: Borislav Angelov

Received: 25 November 2023
Revised: 19 December 2023
Accepted: 22 December 2023
Published: 24 December 2023

1. Introduction

β-xylosidase (4-β-D-xylan xylohydrolase, E.C. 3.2.1.37) is a glycoside hydrolase (GH) catalyzing the hydrolysis of (1→4)-β-D-xylans, allowing for the removal of D-xylose residues from its non-reducing termini. Together with other xylan-degrading enzymes, β-xylosidases are involved in the enzymatic hydrolysis of lignocellulosic biomass [1]. The interest in xylan-degrading enzymes has greatly increased during the last decade due to their potential in a wide range of industrial processes, such as paper pulp bleaching, deinking of recycled paper, enhancement of the digestibility and nutritional properties of animal feed, or clarification of fruit juices ([2] and references therein). Different GH families have been proposed based on their sequence/structure [3], whose classification is regularly updated at the Carbohydrate-Active Enzymes database (CAZy, http://www.cazy.org/ (accessed on 1 November 2023); [4]). On the other hand, different structurally unrelated GH enzymes are grouped under the E.C. 3.2.1.37 classification based on their common activities. In this sense, GH families where β-xylosidase activity has been suggested are as follows: 1, 2, 3, 5, 10, 30, 39, 43, 51, 52, 54 and 120 [5] (GH 11 and GH 116 families also present β-xylosidase activity, according to the CAZY database.). On the other hand, a must-read work on β-xylosidases shows that some of these families might not be active on natural

substrates [2], but only on pNP-derivatives. Despite these controversies, β-xylosidases represent a clear example of the cross-reactivity and classification complexity of GHs [6].

β-xylosidases from the GH52 family of contrasted activity have been found in *Geobacillus* [7–11], *Aeromonas* [12], *Halalkalibacterium* [13], *Paenibacillus* [14] or *Thermoanaerobacterium* [15] species. Enzymes from the GH52 family act generally as specific *exo*-β-xylosidases, which can also cleave artificial xylosides and xylooligosaccharides (e.g., *p*-nitrophenyl-β-D-xylopyranoside, 4-nitrophenyl-β-D-glucopyranose, xylobiose or xylotriose [7–9,14,16]. The β-xylosidases from *Geobacillus stearothermophilus* T-6 or *Aeromonas caviae* also showed low levels of activity towards α-L-arabinofuranoside [9,12]. A retaining mechanism has been proposed to prevail in the GH52 family [7]. Transglycosylation activity has also been observed in this family, as for other GHs [17]. Protein Engineering has been explored on the GH52 scaffold, allowing the introduction/improvement of xylanase [18] or glycosynthase activities [19]. A mutant form of XynB2 from *Geobacillus stearothermophilus* CECT43 also proved useful as an immobilized biocatalyst, such as cross-linked enzyme aggregates or covalently immobilized enzymes, resulting in pH stability and thermostability improvement of the biocatalyst [20,21]. These results suggest that β-xylosidase might be a good candidate for the generation of cross-linked enzyme crystals [22], for which protein crystallization is a mandatory pre-requisite.

The study of protein structures is necessary to understand the molecular principles of protein activity or for the design of enzymes with evolved properties [23]. From the structural point of view, only the 3D model of the GH52 β-xylosidase from *Parageobacillus* (*Geobacillus*) *thermoglucosidasius* NBRC 107,763 has been described in some detail (GthXynB2, PDBs 4C1O and 4C1P [16]). The structure of the catalytic mutant XynB2-E335G from *Geobacillus stearothermophilus* T6 (GstT6XynB2-E335G) is also available at the PDB (PDB 4RHH), but only a crystallization report is available for this enzyme [24]. Structural similarities found between the GH52 and GH116 families suggested their aggrupation under clan GH-O [25]. Based on the limited structural information on GH52 members, we embarked on the crystallization and structural resolution of the XynB2 from *Geobacillus stearothermophilus* CECT43 (Gst43XynB2, 86.24% and 99% sequence similarity with GthXynB2 and GstT6XynB2, respectively). We have determined its crystallization conditions and solved its structure at 2.25 Å, providing a new structural example for the poorly described GH52 family. Based on our results, we propose the existence of a dynamic loop closing the entrance of the catalytic cleft. Structural similarities between the GH52 and GH116 families shed light on the glycone specificity at the −1 binding site.

2. Materials and Methods

2.1. Cloning, Expression and Purification of Gst43XynB2

The cloning, expression and purification of Gst43XynB2 were previously described [10]. Briefly, β-xylosidase gene was amplified by PCR from *Geobacillus stearothermophilus* CECT 43 and cloned into pBluescript II SK (+) plasmid (pBSK, Stratagene Cloning Systems) to create plasmid pJAVI91 (GenBank Acc. No. WOK24302). *E. coli* BL21 DE3 C43/pJAVI91 was grown in a LB medium supplemented with ampicillin. For the induction and expression of the gene, 1 mM IPTG (Isopropyl β-D-1-thiogalactopyranoside) was added to the culture and incubated at 37 °C overnight. After cells disruption by sonication, the recombinant Gst43XynB2 was purified by metal affinity chromatography using TALON cobalt affinity resin (Takara). An additional gel filtration purification step was carried out using 20 mM Tris pH 8.0 as running buffer, using a Superdex 200 column equipped on an Akta prime FPLC. The fractions corresponding to Gst43XynB2 were pooled and concentrated using an Amicon Ultra-Millipore centrifugation system (30 kDa cut-off) up to 17–19 $mg \cdot mL^{-1}$ at 4 °C. Protein purity was verified by SDS-PAGE, and concentration was determined spectrophotometrically at 280 nm using the theoretically calculated extinction coefficient of 136,710 $M^{-1} \cdot cm^{-1}$. Gst43XynB2 was stored at 4 °C for further crystallization experiments.

2.2. Activity Measurements

Activity of Gst43XynB2 was assayed spectrophotometrically as previously described using the chromogenic substrate 4-nitrophenyl β-D-xylopyranoside (pNPX), measuring the release of para-nitrophenol (pNP) at 410 nm [10]. The hydrolysis of 2 mM p-NPX was measured using 50 nM of purified Gst43XynB2 (100 mM Na_2HPO_4 buffer pH 6.5, 50 °C, 5 min). The reaction was stopped by the addition of 1 M Na_2CO_3. An extinction coefficient of $\Delta\varepsilon$ = 18 mM^{-1} cm^{-1} was used for pNP [20,21]. Glycerol inhibition was tested to concentrations of up to 50% (*v*:*v*).

2.3. Thermal Shift Assays

Thermal shift assays (TSA) were carried out on a QuantStudio 3 qPCR (Applied Biosystems, Thermo Fisher, Madrid, Spain). Thermal denaturation was monitored by measuring changes in the fluorescence as a result of SYPRO binding. Thermal unfolding curves were collected from 25 to 99 °C (scan rate 3 °C·min^{-1}). Three replicates were conducted in all cases (SYPRO final concentration 12×). Thermal denaturation of Gst43XynB2 (1.0 mg·mL^{-1}) was assayed in different 50 mM buffers (acetate, phosphate, Tris and carbonate; pHs 4.0–10.4). Apparent thermal denaturation midpoints (T_m^{app}) were calculated using the Protein Thermal Shift Software 1.3 (Applied Biosystems, Thermo Fisher), adjusting the data to the Boltzmann equation. Since the temperature melts were irreversible, the T_m^{app} values should be only considered as a qualitative measurement.

2.4. Crystallization

Freshly purified Gst43XynB2 at a concentration of 17 mg·mL^{-1} was used to perform an initial screening using the counter-diffusion method at 20 °C (Triana kits, Triana Science and Technology [26]), with 0.2 mm inner diameter capillaries. Optimization was carried out using the same configuration, using Gst43XynB2 at a concentration of 8 mg·mL^{-1}. Well-faceted crystals suitable for X-ray diffraction were obtained using 4 M $(NH_4)_2SO_4$ 0.1 M sodium acetate, pH 5.0.

2.5. Data Collection and Refinement

Target crystals were identified under a microscope using polarized light. The selected Gst43XynB2 crystals were drawn from the capillaries and transferred to a 5 µL drop of mother solution containing 15% (*v*/*v*) glycerol as cryo-protectant. After soaking for less than 60 s, crystals were flash-cooled in liquid nitrogen prior to data collection. X-ray diffraction data were collected at ID30B (ESRF, Grenoble, France) and XALOC (ALBA, Barcelona, Spain) beamlines. Diffraction frames were indexed and integrated with XDS [27], and reduced and merged with Aimless [28]. The crystal structure of XynB2 was determined by the molecular replacement method using Molrep [29] from the CCP4 suite [30]. Refinement was carried out with REFMAC [31] and Phenix.refine [32] from the CCP4 [30] and Phenix suites [33]. Manual rebuilding and water inspection were carried out using COOT [34] and finalized including several cycles of refinement applying TLS parameterization [35]. Model quality was followed with Molprobity [36] set-up within the PHENIX package [33]. Data collection and refinement statistics are summarized in Table 1.

Table 1. Data collection and refinement statistics. Statistics for the highest-resolution shell are shown in parentheses.

PDB ID.	8QME
Beam Line	ID30B (ESRF)
Data collection	
Resolution range (Å)	81.67–2.25 (2.33–2.25)
Space group	P 1

Table 1. *Cont.*

Unit cell	
a, b, c (Å)	81.12, 97.51, 107.40
α, β, γ (°)	107.46, 98.48, 106.55
Unique reflections	134,247 (13,293)
Multiplicity	1.8 (1.7)
Completeness (%)	97.17 (96.23)
Mean I/sigma (I)	5.23 (1.31)
Wilson B-factor	32.14
R-merge	0.09505 (0.5006)
CC1/2	0.985 (0.604)
Refinement	
R-work/R-free (%)	17.79/21.29
Number of atoms	
Protein	22,179
Ligands	161
Solvent	1499
Bond lengths (Å)	0.003
Bond angles (°)	0.57
Ramachandran (%)	
favoured	97.46
allowed	2.54
outliers	0.00
B-factor (Å^2)	35.56

2.6. Sequence and Structural Analyses

Sequence alignment was carried out with Clustal W [37] and ESPript [38]. Dali server [39] was used to search for Gst43XynB2 homologs. The PISA server was used to calculate probable assemblies of different protein structures [40]. PDBsum server was used to determine interactions between the different subunits of dimeric structures [41]. Graphical representation and comparison of 3D structural models were carried out with PyMol [42] and Swiss-PdbViewer [43]. Superposition of GH52 and GH116 structures was conducted with the program LSQKAB from the CCP4 suite [44]. Molecular Dynamics simulations were carried out with the CABS-flex 2.0 server [45].

3. Results and Discussion

3.1. Gst43XynB2 Purification and Crystallization

Gst43XynB2 was purified in soluble form in sufficient purity and quantity for crystallization (Figure 1A), with an apparent molecular mass of ~80 kDa, very similar to that deduced from its amino acid sequence (80.66 kDa). TSA experiments showed the highest T_m^{app} at pH 8.0 (Figure 1B), suggesting this pH is optimal for enzyme storage and crystallization set-up. A protein sample (17 mg·mL^{-1} in 20 mM Tris pH 8.0) was used to determine crystallization conditions against Triana kit screenings (CSK24, AS and PPP) using the counter-diffusion method, using 0.2 mm capillaries. Initial crystals were obtained using MixPEG 100 mM Tris pH 7.0 and 4 M $(NH_4)_2SO_4$ 100 mM sodium acetate pH 5.0. Optimization was carried out by decreasing Gst43XynB2 concentration (8 mg·mL^{-1}). Well-faceted crystals suitable for X-ray diffraction were obtained using 4 M $(NH_4)_2SO_4$ 100 mM sodium acetate, pH 5.0 (Figure 1C).

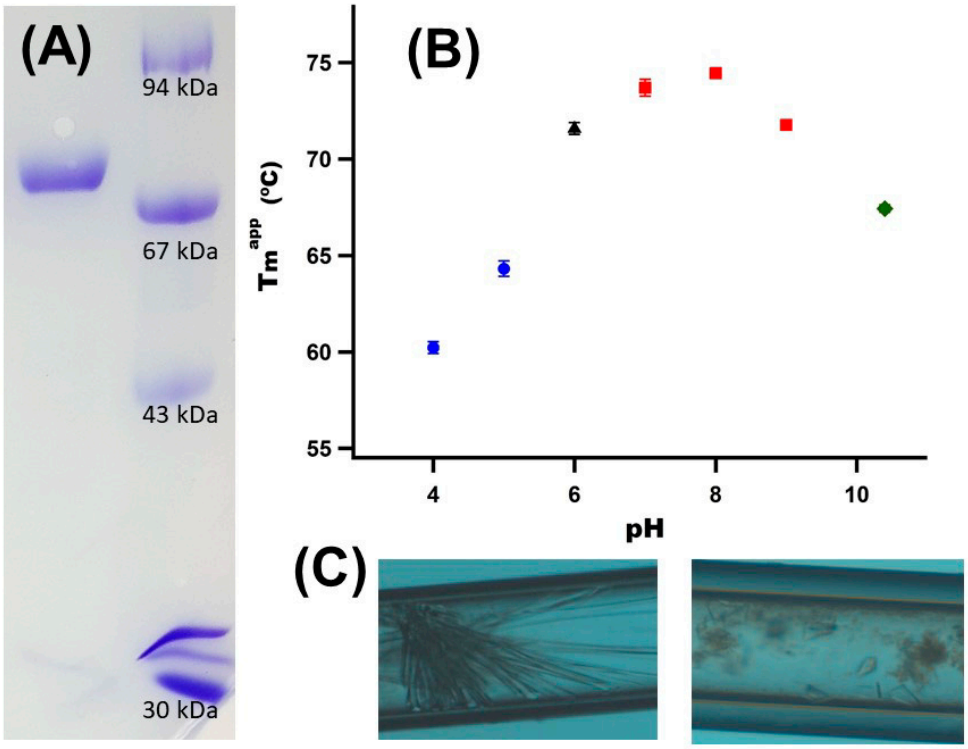

Figure 1. Purification, characterization and crystallization of Gst43XynB2. (**A**) SDS-PAGE of recombinant Gst43XynB2. (**B**) Effects of pH on Gst43XynB2 apparent thermal denaturation midpoints ($T_m{}^{app}$, blue circles, 50 mM acetate buffer; black triangle, 50 mM phosphate buffer; red square, 50 mM Tris buffer; green diamond, 50 mM carbonate buffer). (**C**) Crystals of Gst43XynB2 obtained by the counter-diffusion technique in MixPEG 100 mM Tris pH 7.0 (**left**) and 4 M $(NH_4)_2SO_4$ 100 mM sodium acetate pH 5.0 (**right**).

3.2. Gst43XynB2 Overall Fold

Gst43XynB2 crystal belongs to the triclinic space group P1 and diffracted to 2.25 Å (Table 1). The protomer of Gst43XynB2 is composed of two domains (Figure 2A). An N-terminal domain (residues 1–300) is formed by a central β-sandwich, surrounded by short α-helixes recalling an α-β-β-α sandwich (Figure 2C). Region 65–84 from the N-terminal domain could not be modelled into the structure due to the absence of clear electron density maps. The second domain consists of a distorted C-terminal α/α_6 barrel (approx. residues 300-end; Figure 2B), whose bottom part (end of α-helixes) is completely exposed to the solvent. The catalytic domain (α/α_6 barrel) is decorated with numerous loops and β-hairpins connecting the different α-helixes (Figure 2A,B). As already highlighted [16], the C-terminal domain of Gst43XynB2 constitutes the catalytic domain of the enzyme. Key catalytic residues are placed into the α/α_6 barrel, located in the upper side of the inner α_6 barrel of Gst43XynB2 (Figure 2B).

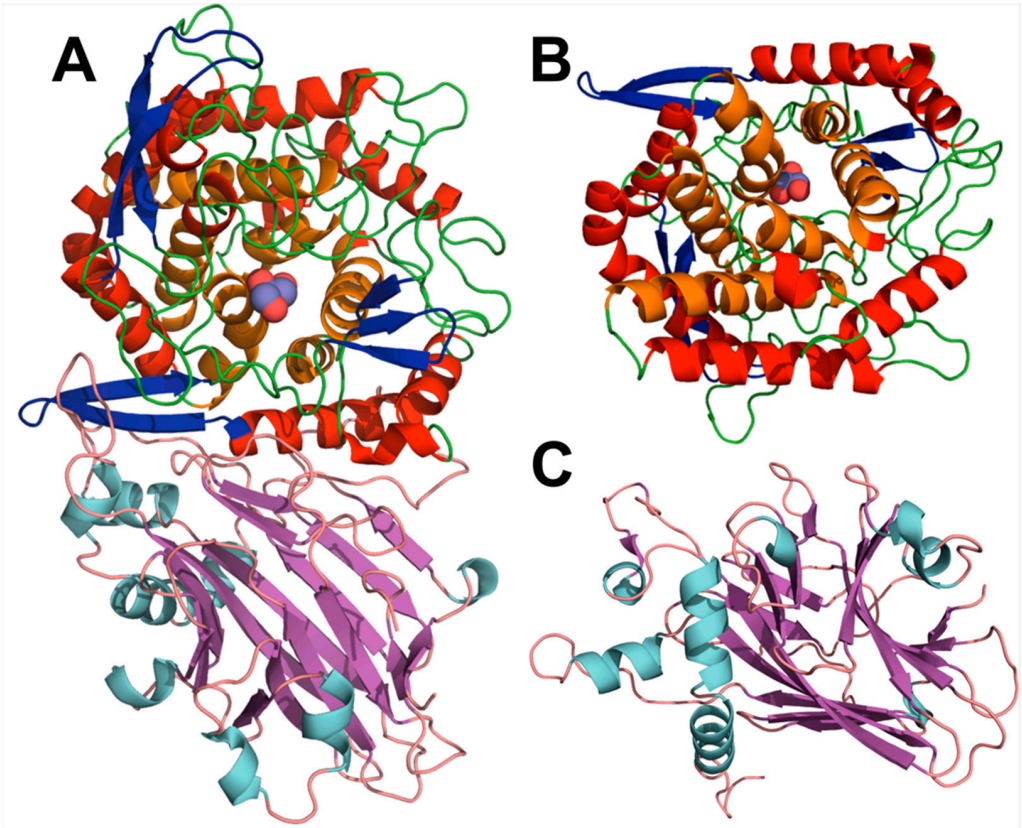

Figure 2. Overall structure of Gst43XynB2 monomer. (**A**) Monomeric structure showing the N-terminal β-sandwich domain (residues 1–300, dimerization domain, cyan and purple) and the distorted C-terminal α/α_6 barrel (residues 300-end, catalytic domain, red, orange, and dark blue). (**B**) Representation of the isolated catalytic domain of Gst43XynB2. The inner α_6 barrel is represented in orange, and the external α_6 barrel in red. β-hairpins/loops inserted into the α/α_6 barrel (319–333, 373–394, 679–687) are shown in blue. A glycerol molecule (shown as spheres) could be fitted into the catalytic centre. (**C**) Representation of the isolated N-terminal domain of Gst43XynB2 where the α-helixes (cyan) surrounding the β-sandwich (purple) can be appreciated.

3.3. Insights into the Dimerization Interface of the GH52 Family

Protein oligomerization is known to play a central role in metabolism and/or protein evolution [46]. Controlled self-assembly is often related to an increase in enzyme thermostability [47], and has been shown to be necessary in the activity of different GH families [48,49]. Gst43XynB2 showed a dimeric rearrangement in solution [10], as has been found for other *Geobacillus* [7,11] or *Aeromonas* xylosidases [12]. No information is available regarding *B. halodurans*, *Paenibacillus* sp., or *Thermoanaerobacterium saccharolyticum* xylosidases [13–15]. Based on the dimeric arrangement of different xylosidases, we wanted to get insights into the structural elements causing the dimerization of Gst43XynB2, trying to understand whether oligomerization has any functionality in the GH52 family. The dimeric rearrangement observed in the crystal structure is calculated as stable (chains A–D) using the EBI PISA server [40], where two rotated molecules face their C- and N-termini (Figure 3A). The superposition of the Gst43XynB2 protomers resulted in an RMSD of 0.69 Å for all the atoms. The superposition of the dimeric structures of Gst43XynB2 with GthXynB2 (PDB 4C1P) and GstT6XynB2-E335G (PDB 4RHH) resulted in an RMSD of 0.49 and 0.41 Å, using only the backbone atoms (1365 and 1361 atoms, respectively).

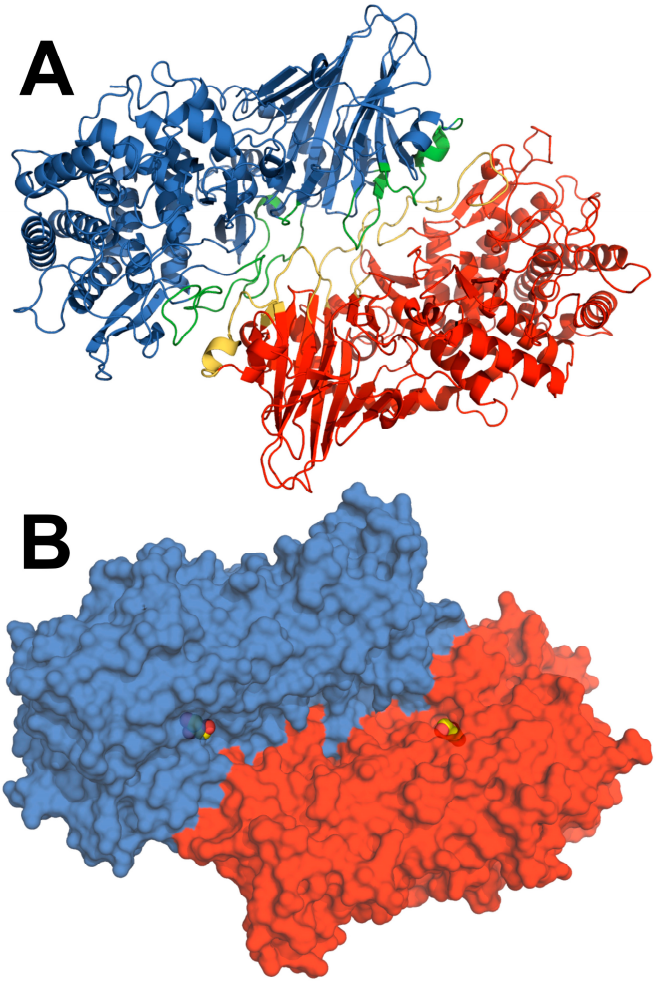

Figure 3. Dimeric arrangement of Gst43XynB2. (**A**) Overall Gst43XynB2 dimer showing the position of structural elements involved in oligomer formation (regions 164–172, 215–226, 249–263 and 400–420; shown in green and yellow). (**B**) Surface representation of the dimeric Gst43XynB2. The position of a glycerol molecule into the catalytic centre is shown in sphere mode.

The contact interface of the dimeric Gst43XynB2 consists of 38 and 39 residues from chains A and D, respectively. The majority of the interface arises from 22 direct hydrogen bonds and 222 non-bonded contacts, covering an approximate area of 2000 Å^2. These contacts arise mostly from residues in loops connecting secondary structure elements located in the N-terminal domain (regions 164–172, 215–226, 249–263), but also some from the α/α_6 barrel (region 400–420) (Figures 3A and S1). The catalytic cleft is situated at the end of a wide intersubunit channel (Figure 3B).

A reciprocal salt bridge appears in the interface of the Gst43XynB2 N-terminal domain (Arg189-Asp259), also observed in GstT6XynB2-E335G (PDB 4RHH) and GthXynB2 (PDB 4C1P and 4C1O). This salt bridge is most likely related to the dimerization of the enzyme. GstT6XynB2-E335G presented reciprocal salt bridges between Arg37-Glu76 and Arg40-Glu76, whereas GthXynB2 presented only the counterpart Arg60-Glu98 salt bridge. The counterpart Glu76^{Gst43XynB2} is placed in the unfitted loop in the Gst43XynB2 structure, avoiding direct identification of this salt bridge. Interestingly, different conformations are found for the Arg residues binding to Glu76$^{GstT6XynB2\text{-}E335G}$/Glu90^{GthXynB2}. Sequence alignment of Gst43XynB2 with other β-xylosidases reviewed in the CAZY database showed total conservation of Arg189 and Asp259 (Figure S2, 44.8–98.9% seq. id.). Glu76 is also totally conserved, and a high conservation of Arg37 is shown (a Lys appears only in *Aeromonas* species). Arg40 is less conserved, with Lys, Asp or Glu residues also appearing in this

position. Nonetheless, as it will be discussed below, the Arg37/Arg40/Glu76 interaction might be important for the catalysis of Gst43XynB and other GH52 family members.

3.4. Comparison of GstXynB2 Structures Suggests the Involvement of a Dynamic Loop in Catalytic Cleft Closure

By analogy with other GH enzymes, two different binding sites were identified in the GH52 superfamily (−1 and +1), one for each of the sugar moieties of a disaccharide ([16], Table S1). GthXynB2 and GstT6XynB2-E335G structures presented ligands bound to the −1 binding site (Tris and glycerol, respectively, Figure 4B,C). Electron densities compatible with a ligand into the −1 binding site of Gst43XynB2 were also observed. Glycerol was previously suggested as a competitive inhibitor of GthXynB2, although no data was provided [16]. We confirmed glycerol inhibition of Gst43XynB2, but only at very high concentrations (53% remaining activity using 50% glycerol). Since glycerol was used as a cryoprotectant for Gst43XynB2 crystals, this molecule was fitted in the −1 binding site of our structure. It showed at binding distance of Glu335, Asp345, His396, Thr493 and Arg693 (Figure 4A, Table S1).

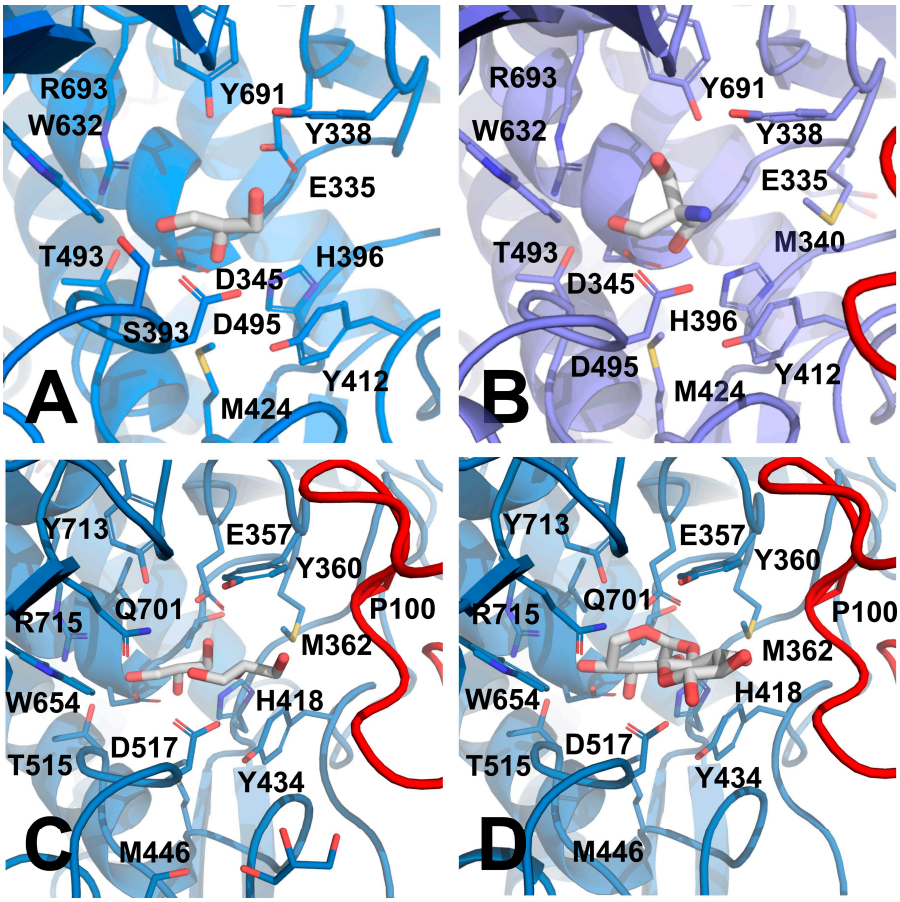

Figure 4. Ligand binding observed for the different X-ray structures available for GH52 members. (**A**) Glycerol molecule bound into the −1 site in Gst43XynB2. (**B**) Tris molecule bound to GstT6XynB2-E335G (PDB 4RHH). (**C**) Glycerol (PDB 4C1O) and (**D**) Xylobiose (PDB 4C1P) molecules bound into the −1 and +1 sites in GthXynB2. Loops coming from a second protomer are highlighted in red. The position of the loop containing $Pro78^{GstT6XynB2\text{-}E335G}$ or $Pro100^{GthXynB2}$ closing the catalytic cleft are only shown in (**B**–**D**).

Except for fitting of isolated water molecules, no clear densities could be observed in the Gst43XynB2 +1 binding site (Figure S3, Table S1). Glycerol (PDB 4C1O) or xylobiose (PDB 4C1P) were modelled in the GthXynB2 +1 binding site (Figure 4C,D, Table S1).

The main interaction with xylobiose in the +1 binding site (PDB 4C1P) was proposed through stacking with Tyr360^{GthXynB2} (Figure 4D, [16]). Apart from this plausible parallel-displaced stacking, polar interactions not mentioned before also exist with Gln701^{GthXynB2} (Figure 4D, Table S1). Interactions between glycerol and Asp517^{GthXynB2} and Gln701^{GthXynB2} also appear (Figure 4C, PDB 4C1O, Table S1). Finally, Pro100^{GthXynB2} was suggested to interact with xylobiose through the polypeptide main chain, being the only residue from a second protomer participating in ligand binding (Figure 4D). This interaction would close/complement the +1 site and was suggested to restrict the access to the catalytic cleft, preventing the entry of large xylan polymers [16]. Strikingly, whereas no ligand was fitted in the GstT6XynB2-E335G +1 binding site (PDB 4RHH, Figure 4B), a closer inspection to this structure reveals the presence of extra electron densities, where a glycerol molecule could be fitted (Figure S4). This molecule would be placed at <3.0 Å distance of Pro78$^{GstT6XynB2\text{-}E335G}$ (counterpart of Pro100^{GthXynB2}; Figure S4).

The loop containing Pro100^{GthXynB2}/Pro78$^{GstT6XynB2\text{-}E335G}$ could be modelled in GthXynB2 structures (residues 82–110; PDBs 4C1O and 4C1P, [16]) and partly in GstT6XynB2-E335G structure (PDB 4RHH, residues 61–88; this structure lacks residues 63–73) (Figure 4B–D). B-factors for residues in these loops are roughly over 40 Å^2, much higher than the rest of the structure (Figure S5). The flexibility of this loop is supported by MD simulations (Figure S6). However, we could not model this loop into the Gst43XynB2 structure (residues 65–84, containing Pro78^{Gst43XynB2}), due to the absence of clear electron densities. As it has been mentioned previously, no ligand could be observed in the Gst43XynB2 +1 binding site, and thus, there was no possibility of ligand binding through the polypeptide chain of Pro78^{Gst43XynB2}, as it was observed with GthXynB2 and GstT6XynB2-E335G (Figures 4C,D and S4). These results suggest partial disorder of this region, showing an open conformation in the Gst43XynB2 structure. Altogether, we might argue that this loop is structurally dynamic, and ligand binding would allow the closure of the catalytic cleft, as shown in GthXynB2 and GstT6XynB2-E335G.

Although more experiments are necessary, this loop might act as an unidentified gatekeeper in the GH52 family. The existence of structurally dynamic segments in the entrance/exit to the catalytic cleft of different GH families has been reported (e.g., TfCel5A (GH5, [50]), cellobiohydrolase (GH6, [51]), xylanase (GH11, [52]), chitinase, (GH18, [53]) or galacto-N-biose/lacto-N-biose I phosphorylase (GH112, [54]). The plausible anchor for this loop could be one of the identified conserved salt bridges in the dimer interface of GthXynB2 (Arg57^{GthXynB2} and Glu98^{GthXynB2}) and GstT6XynB2-E335G (Arg37^{GstT6XynB2} and Glu76^{GstT6XynB2}).

3.5. Structural Comparison of GH52 and GH116 Family

Espina and co-workers compared the GthXynB2 structure with those of other GH families with proven xylosidase activity available at the PDB at that moment, which also presented reaction mechanisms with retaining product conformation (GH39 and 120; [16]). Apart from the canonical catalytic nucleophile/base and protein donor residues, conservation in the catalytic cleft was very low. These authors also suggested that the presence of the N-terminus from a second monomer in the dimeric GthXynB2 (where Pro100^{GthXynB2} is placed), participating in catalytic cleft closure, resulted in a narrowed substrate entrance. They concluded that this strategy might be an adaptation to restrict access to smaller xylo-oligosaccharides for the GH52 family [16].

More recently, structural similarities between *Thermoanaerobacterium xylanolyticum* β-glucosidase (TxGH116) and GthXynB2 overall folds suggested the aggrupation of GH52 and GH116 families under clan GH-O [25]. The GH116 family has received higher structural attention due to its similarity to β-glucosylceramidase 2, a drug target related to different human pathologies [25,55]. This family has also been profoundly studied from a mechanistic point of view [56,57]. Up to four different subfamilies have been proposed for GH116 [58,59]. However, to date, only two GH116 subfamilies have structures available in

the PDB (*exo*-β-D-arabinofuranosidase (ExoMA2, e.g., PDB 8IC6, [59]) and β-glucosidase (TxGH116, e.g., PDB 5BX5, [25]).

GH52 and GH116 overall topologies consist of a catalytic C-terminal α/α_6 barrel and a N-terminal β-sandwich-based domain, showing different inserted structural elements (the sequence identity is lower than 13% between Gst43XynB2 and ExoMA2 and TxGH116, Figure 5). TheExoMA2 fold also presents an additional C-terminal β-sandwich domain, closing the bottom of the catalytic centre, suggesting further structural divergence. ExoMA2 is also a dimer in solution [59], although the dimerization interface is different between the GH52 and the GH116 family (Figure S7). TxGH116 oligomerization showed a more complex scenario, showing monomeric, dimeric, and oligomeric species in solution, with dimeric being suggested as the major form [25]. In conclusion, oligomerization, most likely dimerization, seems to be a common structural feature for these clan GH-O members.

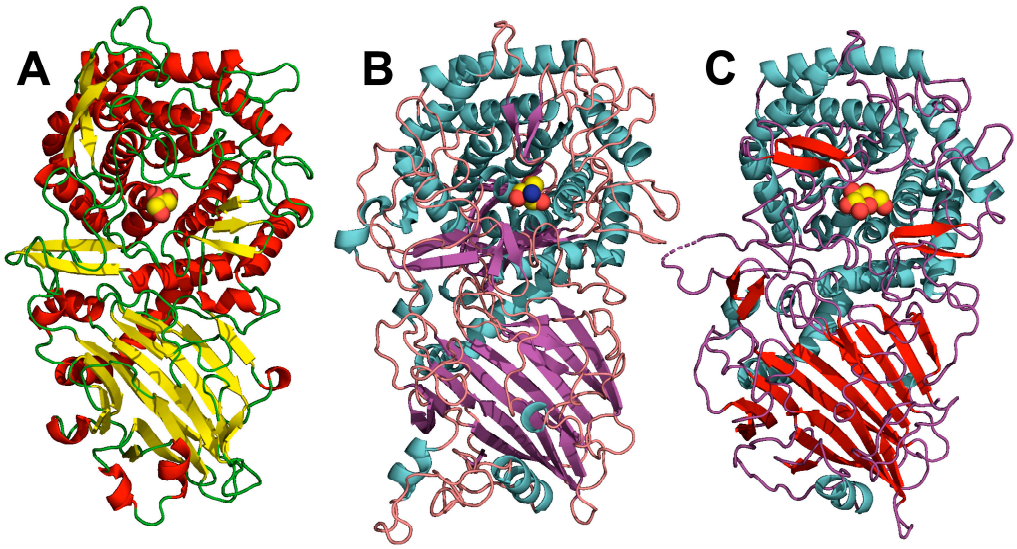

Figure 5. Overall structures of GH52 and GH116 family representatives. (**A**) Gst43XynB2 (PDB 8QME). (**B**) β-Glucosidase TxGH116 (PDB 5BX5). (**C**) *exo*-β-D-Arabinofuranosidase ExoMA2 (PDB 8IC7). Ligands found in the catalytic sites of each structure are represented in ball mode.

Expected similarities were found when comparing the catalytic centres of Gst43XynB2, ExoMA2, and TxGH116, with the catalytic nucleophile/base and proton donor identical in the GH52/GH116 structures (Table 2). Several residues were conserved when compared to ExoMA2, but a striking and higher similarity was found among GstXynB2 and TxGH116. The superposition of Gst43XynB2 and TxGH116 structures through the conserved residues in the catalytic α/α_6 barrel showed a clear correspondence between most of the residues in the −1 site (Figure 6, Table 2). A higher divergence was observed at the +1 site (Figure S8, Table 2). Specifically, two of the loops containing residues forming the +1 site in the GH52 family are not conserved among the different structures. First, a low conservation was observed between loops 440–444^{GthXynB2} (420–424^{Gst43XynB2}) and 524–528^{TxGH116} from the +1 site; this loop is absent in ExoMA2. Loop 524–528^{TxGH116} is covered by a β-hairpin, which also appears in the GH52 family but is totally displaced between the two structures (residues 480–504^{TxGH116}/373–395^{Gst43XynB2}, Figure S9). Secondly, the mobile segment found in the GH52 family coming from a second monomer (where Pro100^{GthXynB2} is placed (Pro78^{Gst43XynB2}), see above), belongs to the own monomer in TxGH116 (loop 60–65^{TxGH116}, Figure S8). The counterpart loop in ExoMA2 is shorter (region 80–88) and does not cover the catalytic entrance, which is further exposed to the solvent. Whereas no involvement in the activity or ExoMA2 or TxGH116 of residues from the +1 site, nor from a second protomer, were depicted previously [25,59], additional loops from the second monomer are placed on this region for ExoMA2 (e.g., loop 226–237, Figure S8). These loops also present

high B-factors in the corresponding structure (regions 226–237; 249–293). However, at this point, it is unclear whether dimerization is needed for TxGH116 or ExoMA2 activity.

Table 2. Residue conservation in the −1 and +1 site of different members of the GH52 and 116 families.

Gst43XynB2	GthXynB2	TxGH116	ExoMA
PDB 8QME	**PDB 4C1P**	**PDB 5BX5**	**PDB 8IC7**
Glu335	Glu357	Glu441	Glu431
Tyr338	Tyr360	Tyr445	Ser439/Cys440
Met340	Met362	Tyr447 *	Cys440/Glu441/Cys758 *
Thr343	Thr365	Thr450	Cys444
Asp345	Asp367	Asp452	His445
Leu346	Leu368	Val453	Val447
His396	His418	His507	Phe482/Arg483 *
Tyr412	Tyr434	Tyr523	---
Cys420/Phe421	Cys442/Phe443	Trp525	Trp234 *
Met424	Met446	Trp531	Ala498
Thr493	Thr515	Thr591	Thr555
Tyr494	Tyr516	Tyr592	Tyr556
Asp495	Asp 517	Asp593	Asp557
Ser496	Ser518	Thr594 *	Tyr709 *
Trp632	Trp654	Trp732	Trp714
Gln679	Gln701	Arg786 *	Arg682 *
Ser688	Ser710	Ala787 *	Glu757/Cys758 *
Tyr691	Tyr713	Tyr790	Tyr762
Arg693	Arg715	Arg792	Arg764

* These residues do not occupy exactly the same position (loops displaced, belonging to a different structural element, protomer, etc.).

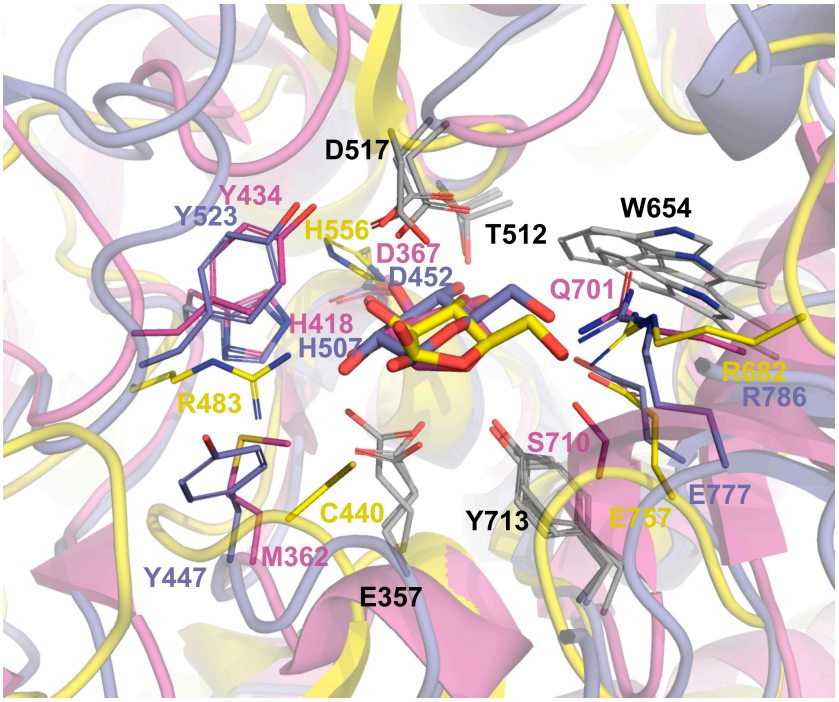

Figure 6. Superposition of the −1 binding site of GthXynB2 (PDB 4C1P, pink tones), TxGH116 (PDB 5BX5, blue tones) and ExoMA2 (PDB 8IC7, yellow tones). Residues differing between the three structures are shown in the same color as the corresponding structure. Residues totally conserved between the three structures are marked in gray for clearness, and only the name of the residue from GthXynB2 is shown (in black). Residue correspondence between the different structures can be consulted in Tables 2 and S1.

3.6. Insigths into the Glycone Specificity (−1 site) of GH52 and GH116 Families

GHs are often highly specific with regard to the identity of the substrate glycone, which occupies the −1 binding site [8,9]. However, cross-reactivity is also a common feature within GHs, also shown within the GH52 family members; as way of example, despite showing a clear preference for 4-nitrophenyl β-D-xylopyranoside (4NPβ-D-xyl), GstT6XynB2 proved active towards different unnatural 4-nitrophenyl glycosides (4-NPGs), including 4-nitrophenyl β-D-glucopyranoside (4NPβ-D-glu, [8]). k_{cat} values varying more than two orders of magnitude proved determinant for the catalityc efficiency of this enzyme towards different 4-NPGs. However, GstT6XynB2 showed similar K_m values for other 4-NPGs to that of 4NPβ-D-xyl, ascertaining that it was able to bind different glycones with similar affinities. With regard to GH116 family, at least three members have shown activity towards 4NPβ-D-xyl. The first one was SSO1353, classified as a bifunctional aryl β-glucosidase/β-xylosidase. This enzyme showed catalytic efficiency in the same order for xyloside and glucose derivatives [60]. The second member, SSO3039, was proposed as a bifunctional *exo*-β-glucosidase/N-acetyl-β-glucosaminidase [58]. Finally, TxGH116 was proposed as a β-glucosidase [61] (although no activity was observed towards this compound in [62]). On the other hand, no activity was detected with ExoMA2 towards pNP-β-D-Glcp or pNP-β-D-Xylp, suggesting a high specificity for pNP-β-D-Araf [59].

As explained above, the −1 binding site for GstXynB2 (since the catalytic centers of the three structures for GthXynB2, Gst43XynB2 and GstT6XynB2 are totally conserved (see Table S1), we will refer to GstXynB2 when it is not necessary to mention specifically one of them.) and TxGH116 is structurally more similar than that of ExoMA2 (Figure 6, Table 2). $Glu777^{TxGH116}$ and $Arg786^{TxGH116}$ are at the binding distance of the C6-hydroxymethyl group of the β-glucose glycone of cellobiose (Figure 6). Similarly, $Glu757^{ExoMA2}$ and $Arg682^{ExoMA2}$ are used by ExoMA2 to bind the C5-hydroxymethyl arabinose group, although these residues come from different structural loops (Figure 6). No exact counterpart in GstXynB2 exists, but this region is occupied by $Gln701^{GthXynB2}$ ($Gln679^{Gst43XynB2}$) and $Ser710^{GthXynB2}$ ($Ser688^{Gst43XynB2}$), at the binding distance of the xylose glycone of xylobiose (Figure 6). $Met362^{GthXynB2}$ ($Met340^{Gst43XynB2}$) is replaced by $Tyr447^{TxGH116}$ or $Cys440^{ExoMA2}$, but these residues are at more than 3.5 Å distance of the ligands in the different structures, and thus, it seems arguable that they do not participate in ligand binding (Figure 6). Finally, the major divergence of the ExoMA2 −1 binding site is also shown by $Arg483^{ExoMA2}$ and $His556^{ExoMA2}$, occupying counterpart positions of $His418^{GthXynB2}$ ($His396^{Gst43XynB2}$)/$His507^{TxGH116}$ and $Asp367^{GthXynB2}$ ($Asp345^{Gst43XynB2}$)/$Asp452^{TxGH116}$ (Figure 6); no counterpart residues appear in ExoMA2 for $Tyr434^{GthXynB2}$/$Tyr523^{TxGH116}$. Whereas we are aware that 4-NPG must diffuse into the −1 binding site crossing the +1 site, we might argue that the observed differences in these residues are most likely responsible for the different specificities observed in 4-NPG hydrolysis by GstXynB2, TxGH116, and ExoMA2 [8,59].

4. Conclusions

In this work, we have crystallized Gst43XynB2, providing the second structural description of a member of the GH52 family. Our work suggests a previously unidentified gatekeeper loop in this GH family, which might flap upon ligand binding. These results would also explain the necessity for a dimeric arrangement in the GH52 family, where catalytic cleft closure would occur through this loop, belonging to a second protomer. The Gst43XynB2 structure seems to represent an open conformation, whereas the GthXynB2 and GstT6XynB2-E335G structures would represent a closed conformation. This notion is supported by the existence of other dynamic segments in the entrance/exit to the catalytic cleft of different GH families [50–54]. The plausible anchor for this loop might be one of the conserved salt bridges observed in the interface of GthXynB2 ($Arg57^{GthXynB2}$ and $Glu98^{GthXynB2}$) and GstT6XynB2-E335G ($Arg37^{GstT6XynB2}$ and $Glu76^{GstT6XynB2}$).

From a structural point of view, GH clans are expected to have evolved from a common ancestor. According to our results, divergence from an ancestral clan-O member might have

led to the different specificities found in the GH52 and GH116 families. Our crystallization and structural studies shed light on how conservation of the −1 binding site of GstXynB2 and TxGH116 paves the way to substrate promiscuity over different unnatural 4-NPG substrates (e.g., 4NPβ-D-xyl and 4NPβ-D-glu). Specifically, our structural studies reveal that $Glu777^{TxGH116}$/$Arg786^{TxGH116}$ and $Gln679^{Gst43XynB2}$/$Ser688^{Gst43XynB2}$ are responsible for the preference for a glucosyl- or xylosil- moiety in the −1 binding site in these enzymes. On the other hand, the observed greater divergence of ExoMA2 also explains the different specificity of this enzyme for pNP-β-D-Araf. Although further results are needed, the observed dissimilarity of the +1 binding site would further support evolutionary aspects leading to the different substrate specificities, where GH52 members would have evolved towards specificity on xylooligosacharide derivatives, whereas GH116 members would have specialized towards different glucosyl- (subfamilies 1–3) or arabinosyl- (subfamily 4) substrates (see [58,59] for insights into GH116 subfamilies and specificities).

Supplementary Materials: The following supporting information can be downloaded at: https://www.mdpi.com/article/10.3390/cryst14010018/s1, Figure S1: Contacts found in the Gst43XynB2 interface, as calculated by PDBsum server. Figure S2: Sequence alignment of β-xylosidases of contrasted activity available at the CAZY database. Figure S3: Electron densities in the Gst43XynB2 +1 site contoured at 1.09 σ. Figure S4: Extra densities found in the GstT6XynB2 +1 site. Figure S5: Representation in putty mode of the different *Geobacillus* XynB2 structures. Figure S6: Fluctuation map obtained with the CABS-flex 2.0 server using the GthXynB2 structure as input. Figure S7: Different dimerization interfaces found in the GH52 and the GH116 families, using Gst43XynB2 and ExoMA2 as representatives. Figure S8. Superposition of the +1 binding site of GthXynB2, TxGH116 and ExoMA2. Figure S9: Common β-hairpin appearing in TxGH116 and Gst43XynB2. Table S1: Residues in the different *Geobacillus* XynB2 structures with any atom at less than 4 Å from the ligands found in binding subsites +1 and −1.

Author Contributions: Conceptualization, J.A.G., L.M.C., F.J.L.H.-V. and S.M.-R.; formal analysis, J.A.G., L.M.C., F.J.L.H.-V. and S.M.-R.; investigation, J.A.G., L.M.C., H.M.A., J.M.C.-J., F.J.L.H.-V. and S.M.-R.; resources, J.A.G., S.M.-R., F.J.L.H.-V. and F.R.-V.—original draft preparation, S.M.-R. and J.A.G.; writing—review and editing, S.M.-R., J.A.G., L.M.C., J.M.C.-J. and F.J.L.H.-V.; funding acquisition, J.A.G., F.J.L.H.-V. and F.R.-V. All authors have read and agreed to the published version of the manuscript.

Funding: This research was funded by the Spanish Ministry of Science and Innovation/FEDER funds Grant PID2020-116261GB-I00/AEI/10.13039/501100011033 (JAG), by the European Regional Development Fund Andalucía 2014–2020 Grant UAL18-CTS-B032-A (FRV) and by the Own Research and Transfer Plan 2020 of the University of Almeria Grant PPUENTE2020/006 (FJLHV).

Data Availability Statement: Data available within the article or its Supplementary Materials. Datasets used for structural determination of Gst43XynB2 X-ray diffraction data were collected at ID30B (ESRF, Grenoble, France; https://data.esrf.fr/doi/10.15151/ESRF-ES-541423054, accessed on 1 December 2023). Coordinates and structure factors have been deposited at the PDB with accession code 8QME.

Acknowledgments: We are grateful to the European Synchrotron Radiation Facility (ESRF), Grenoble, France, for providing time through proposal MX2353, and the staff at ID30-A3 beamlines for assistance during data collection. We are also grateful to the Spanish Synchrotron Light Facility (ALBA), Barcelona, Spain, for providing time through proposals 2021085252 and 2022086950, and the staff at XALOC beamline for assistance during data collection. We deeply thank Mª Carmen López-Sánchez for technical assistance. We are grateful to MDPI for their invitation and support of the APCs for this work.

Conflicts of Interest: The authors declare no conflict of interest. The funders had no role in the design of the study; in the collection, analyses, or interpretation of data; in the writing of the manuscript; or in the decision to publish the results.

References

1. Knob, A.; Terrasan, C.R.F.; Carmona, E.C. β-Xylosidases from filamentous fungi: An overview. *World J. Microbiol. Biotechnol.* **2009**, *26*, 389–407. [CrossRef]
2. Rohman, A.; Dijkstra, B.W.; Puspaningsih, N.N.T. β-Xylosidases: Structural Diversity, Catalytic Mechanism, and Inhibition by Monosaccharides. *Int. J. Mol. Sci.* **2019**, *20*, 5524. [CrossRef] [PubMed]
3. Henrissat, B.; Davies, G. Structural and sequence-based classification of glycoside hydrolases. *Curr. Opin. Struct. Biol.* **1997**, *7*, 637–644. [CrossRef] [PubMed]
4. Drula, E.; Garron, M.L.; Dogan, S.; Lombard, V.; Henrissat, B.; Terrapon, N. The carbohydrate-active enzyme database: Functions and literature. *Nucleic Acids Res.* **2022**, *50*, D571–D577. [CrossRef] [PubMed]
5. Kaneko, S.; Fujimoto, Z. Chapter 8-β-D-Xylosidases: Structure-based substrate specificities and their applications. In *Glycoside Hydrolases*; Goyal, A., Kedar, S., Eds.; Academic Press: Cambridge, MA, USA, 2023; pp. 165–186.
6. Nguyen, S.N.; Flores, A.; Talamantes, D.; Dar, F.; Valdez, A.; Schwans, J.; Berlemont, R. GeneHunt for rapid domain-specific annotation of glycoside hydrolases. *Sci. Rep.* **2019**, *9*, 10137. [CrossRef] [PubMed]
7. Bravman, T.; Zolotnitsky, G.; Shulami, S.; Belakhov, V.; Solomon, D.; Baasov, T.; Shoham, G.; Shoham, Y. Stereochemistry of family 52 glycosyl hydrolases: A beta-xylosidase from Bacillus stearothermophilus T-6 is a retaining enzyme. *FEBS Lett.* **2001**, *495*, 39–43. [CrossRef] [PubMed]
8. Bravman, T.; Zolotnitsky, G.; Belakhov, V.; Shoham, G.; Henrissat, B.; Baasov, T.; Shoham, Y. Detailed kinetic analysis of a family 52 glycoside hydrolase: A beta-xylosidase from Geobacillus stearothermophilus. *Biochemistry* **2003**, *42*, 10528–10536. [CrossRef] [PubMed]
9. Bravman, T.; Belakhov, V.; Solomon, D.; Shoham, G.; Henrissat, B.; Baasov, T.; Shoham, Y. Identification of the catalytic residues in family 52 glycoside hydrolase, a beta-xylosidase from Geobacillus stearothermophilus T-6. *J. Biol. Chem.* **2003**, *278*, 26742–26749. [CrossRef]
10. Contreras, L.M.; Gómez, J.; Prieto, J.; Clemente-Jiménez, J.M.; Las Heras-Vázquez, F.J.; Rodríguez-Vico, F.; Blanco, F.J.; Neira, J.L. The family 52 beta-xylosidase from Geobacillus stearothermophilus is a dimer: Structural and biophysical characterization of a glycoside hydrolase. *Biochim. Biophys. Acta* **2008**, *1784*, 1924–1934. [CrossRef]
11. Quintero, D.; Velasco, Z.; Hurtado-Gómez, E.; Neira, J.L.; Contreras, L.M. Isolation and characterization of a thermostable beta-xylosidase in the thermophilic bacterium Geobacillus pallidus. *Biochim. Biophys. Acta* **2007**, *1774*, 510–518. [CrossRef]
12. Suzuki, T.; Kitagawa, E.; Sakakibara, F.; Ibata, K.; Usui, K.; Kawai, K. Cloning, expression, and characterization of a family 52 beta-xylosidase gene (xysB) of a multiple-xylanase-producing bacterium, Aeromonas caviae ME-1. *Biosci. Biotechnol. Biochem.* **2001**, *65*, 487–494. [CrossRef] [PubMed]
13. Teramoto, K.; Tsutsui, S.; Sato, T.; Fujimoto, Z.; Kaneko, S. Substrate Specificities of GH8, GH39, and GH52 β-xylosidases from Bacillus halodurans C-125 Toward Substituted Xylooligosaccharides. *Appl. Biochem. Biotechnol.* **2021**, *193*, 1042–1055. [CrossRef]
14. Lee, T.-H.; Lee, Y.-E. Cloning, Sequencing and Expression of the Gene Encoding a Thermostable β -Xylosidase from Paenibacillus sp. DG-22. *J. Life Sci.* **2007**, *17*, 1197–1203. [CrossRef]
15. Podkaminer, K.K.; Guss, A.M.; Trajano, H.L.; Hogsett, D.A.; Lynd, L.R. Characterization of xylan utilization and discovery of a new endoxylanase in Thermoanaerobacterium saccharolyticum through targeted gene deletions. *Appl. Environ. Microbiol.* **2012**, *78*, 8441–8447. [CrossRef] [PubMed]
16. Espina, G.; Eley, K.; Pompidor, G.; Schneider, T.R.; Crennell, S.J.; Danson, M.J. A novel β-xylosidase structure from Geobacillus thermoglucosidasius: The first crystal structure of a glycoside hydrolase family GH52 enzyme reveals unpredicted similarity to other glycoside hydrolase folds. *Acta Crystallogr. D Biol. Crystallogr.* **2014**, *70*, 1366–1374. [CrossRef]
17. Romero-Téllez, S.; Lluch, J.M.; González-Lafont, À.; Masgrau, L. Comparing Hydrolysis and Transglycosylation Reactions Catalyzed by. *Front. Chem.* **2019**, *7*, 200. [CrossRef] [PubMed]
18. Huang, Z.; Liu, X.; Zhang, S.; Liu, Z. GH52 xylosidase from Geobacillus stearothermophilus: Characterization and introduction of xylanase activity by site-directed mutagenesis of Tyr509. *J. Ind. Microbiol. Biotechnol.* **2014**, *41*, 65–74. [CrossRef] [PubMed]
19. Ben-David, A.; Shoham, G.; Shoham, Y. A universal screening assay for glycosynthases: Directed evolution of glycosynthase XynB2(E335G) suggests a general path to enhance activity. *Chem. Biol.* **2008**, *15*, 546–551. [CrossRef]
20. Romero, G.; Contreras, L.M.; Aguirre, C.; Wilkesman, J.; Clemente-Jiménez, J.M.; Rodríguez-Vico, F.; Las Heras-Vázquez, F.J. Characterization of Cross-Linked Enzyme Aggregates of the Y509E Mutant of a Glycoside Hydrolase Family 52 β-xylosidase from. *Molecules* **2021**, *26*, 451. [CrossRef]
21. Romero, G.; Contreras, L.M.; Aguirre Céspedes, C.; Wilkesman, J.; Clemente-Jiménez, J.M.; Rodríguez-Vico, F.; Las Heras-Vázquez, F.J. Efficiency Assessment between Entrapment and Covalent Bond Immobilization of Mutant β-Xylosidase onto Chitosan Support. *Polymer* **2023**, *15*, 3170. [CrossRef]
22. Kubiak, M.; Kampen, I.; Schilde, C. Structure-Based Modeling of the Mechanical Behavior of Cross-Linked Enzyme Crystals. *Crystals* **2022**, *12*, 441. [CrossRef]
23. Timofeev, V.; Samygina, V. Protein Crystallography: Achievements and Challenges. *Crystals* **2023**, *13*, 71. [CrossRef]
24. Dann, R.; Lansky, S.; Lavid, N.; Zehavi, A.; Belakhov, V.; Baasov, T.; Dvir, H.; Manjasetty, B.; Belrhali, H.; Shoham, Y.; et al. Preliminary crystallographic analysis of Xyn52B2, a GH52 β-D-xylosidase from Geobacillus stearothermophilus T6. *Acta Crystallogr. F Struct. Biol. Commun.* **2014**, *70*, 1675–1682. [CrossRef] [PubMed]

25. Charoenwattanasatien, R.; Pengthaisong, S.; Breen, I.; Mutoh, R.; Sansenya, S.; Hua, Y.; Tankrathok, A.; Wu, L.; Songsiriritthigul, C.; Tanaka, H.; et al. Bacterial β-Glucosidase Reveals the Structural and Functional Basis of Genetic Defects in Human Glucocerebrosidase 2 (GBA2). *ACS Chem. Biol.* **2016**, *11*, 1891–1900. [CrossRef] [PubMed]
26. González-Ramírez, L.A.; Ruiz-Martínez, C.R.; Estremera-Andújar, R.A.; Nieves-Marrero, C.A.; García-Caballero, A.; Gavira, J.A.; López-Garriga, J.; García-Ruiz, J.M. Efficient Screening Methodology for Protein Crystallization Based on the Counter-Diffusion Technique. *Cryst. Growth Des.* **2017**, *17*, 6780–6786. [CrossRef]
27. Kabsch, W. XDS. *Acta Crystallogr. Sect. D Biol. Crystallogr.* **2010**, *66*, 125–132. [CrossRef]
28. Evans, P.R.; Murshudov, G.N. How good are my data and what is the resolution? *Acta Crystallogr. Sect. D Biol. Crystallogr.* **2013**, *69*, 1204–1214. [CrossRef]
29. Vagin, A.; Teplyakov, A. Molecular replacement with MOLREP. *Acta Crystallogr. Sect. D Biol. Crystallogr.* **2010**, *66*, 22–25. [CrossRef]
30. Winn, M.D.; Ballard, C.C.; Cowtan, K.D.; Dodson, E.J.; Emsley, P.; Evans, P.R.; Keegan, R.M.; Krissinel, E.B.; Leslie, A.G.; McCoy, A.; et al. Overview of the CCP4 suite and current developments. *Acta Crystallogr. Sect. D Biol. Crystallogr.* **2011**, *67*, 235–242. [CrossRef]
31. Murshudov, G.N.; Skubák, P.; Lebedev, A.A.; Pannu, N.S.; Steiner, R.A.; Nicholls, R.A.; Winn, M.D.; Long, F.; Vagin, A.A. REFMAC5 for the refinement of macromolecular crystal structures. *Acta Crystallogr. Sect. D Biol. Crystallogr.* **2011**, *67*, 355–367. [CrossRef]
32. Afonine, P.V.; Grosse-Kunstleve, R.W.; Echols, N.; Headd, J.J.; Moriarty, N.W.; Mustyakimov, M.; Terwilliger, T.C.; Urzhumtsev, A.; Zwart, P.H.; Adams, P.D. Towards automated crystallographic structure refinement with phenix.refine. *Acta Crystallogr. Sect. D Biol. Crystallogr.* **2012**, *68*, 352–367. [CrossRef] [PubMed]
33. Liebschner, D.; Afonine, P.V.; Baker, M.L.; Bunkóczi, G.; Chen, V.B.; Croll, T.I.; Hintze, B.; Hung, L.W.; Jain, S.; McCoy, A.J.; et al. Macromolecular structure determination using X-rays, neutrons and electrons: Recent developments in Phenix. *Acta Crystallogr. Sect. D Struct. Biol.* **2019**, *75*, 861–877. [CrossRef] [PubMed]
34. Emsley, P.; Lohkamp, B.; Scott, W.G.; Cowtan, K. Features and development of Coot. *Acta Crystallogr. Sect. D Biol. Crystallogr.* **2010**, *66*, 486–501. [CrossRef] [PubMed]
35. Painter, J.; Merritt, E.A. Optimal description of a protein structure in terms of multiple groups undergoing TLS motion. *Acta Crystallogr. Sect. D Biol. Crystallogr.* **2006**, *62*, 439–450. [CrossRef] [PubMed]
36. Chen, V.B.; Arendall, W.B.; Headd, J.J.; Keedy, D.A.; Immormino, R.M.; Kapral, G.J.; Murray, L.W.; Richardson, J.S.; Richardson, D.C. MolProbity: All-atom structure validation for macromolecular crystallography. *Acta Crystallogr. Sect. D Biol. Crystallogr.* **2010**, *66*, 12–21. [CrossRef] [PubMed]
37. Madeira, F.; Park, Y.M.; Lee, J.; Buso, N.; Gur, T.; Madhusoodanan, N.; Basutkar, P.; Tivey, A.R.N.; Potter, S.C.; Finn, R.D.; et al. The EMBL-EBI search and sequence analysis tools APIs in 2019. *Nucleic Acids Res.* **2019**, *47*, W636–W641. [CrossRef]
38. Robert, X.; Gouet, P. Deciphering key features in protein structures with the new ENDscript server. *Nucleic Acids Res.* **2014**, *42*, W320–W324. [CrossRef]
39. Holm, L. DALI and the persistence of protein shape. *Protein Sci.* **2020**, *29*, 128–140. [CrossRef]
40. Krissinel, E.; Henrick, K. Inference of macromolecular assemblies from crystalline state. *J. Mol. Biol.* **2007**, *372*, 774–797. [CrossRef]
41. Laskowski, R.A.; Jabłońska, J.; Pravda, L.; Vařeková, R.S.; Thornton, J.M. PDBsum: Structural summaries of PDB entries. *Protein Sci.* **2018**, *27*, 129–134. [CrossRef]
42. DeLano, W.L. PyMOL Molecular Graphics System. 2002. Available online: http://www.pymol.org. (accessed on 1 December 2023).
43. Guex, N.; Peitsch, M.C. SWISS-MODEL and the Swiss-PdbViewer: An environment for comparative protein modeling. *Electrophoresis* **1997**, *18*, 2714–2723. [CrossRef] [PubMed]
44. Kabsch, W. A solution for the best rotation to relate two sets of vectors. *Acta Crystallogr. Sect. A Cryst. Phys. Diffr. Theor. Gen. Crystallogr.* **1976**, *32*, 922–923. [CrossRef]
45. Kuriata, A.; Gierut, A.M.; Oleniecki, T.; Ciemny, M.P.; Kolinski, A.; Kurcinski, M.; Kmiecik, S. CABS-flex 2.0: A web server for fast simulations of flexibility of protein structures. *Nucleic Acids Res.* **2018**, *46*, W338–W343. [CrossRef] [PubMed]
46. Gotte, G.; Menegazzi, M. Protein Oligomerization. *Int. J. Mol. Sci.* **2023**, *24*, 10648. [CrossRef] [PubMed]
47. Fraser, N.J.; Liu, J.W.; Mabbitt, P.D.; Correy, G.J.; Coppin, C.W.; Lethier, M.; Perugini, M.A.; Murphy, J.M.; Oakeshott, J.G.; Weik, M.; et al. Evolution of Protein Quaternary Structure in Response to Selective Pressure for Increased Thermostability. *J. Mol. Biol.* **2016**, *428*, 2359–2371. [CrossRef] [PubMed]
48. Wilkens, C.; Vuillemin, M.; Pilgaard, B.; Polikarpov, I.; Morth, J.P. A GH115 α-glucuronidase structure reveals dimerization-mediated substrate binding and a proton wire potentially important for catalysis. *Acta Crystallogr. Sect. D Struct. Biol.* **2022**, *78*, 658–668. [CrossRef]
49. McAndrew, R.P.; Park, J.I.; Heins, R.A.; Reindl, W.; Friedland, G.D.; D'haeseleer, P.; Northen, T.; Sale, K.L.; Simmons, B.A.; Adams, P.D. From soil to structure, a novel dimeric β-glucosidase belonging to glycoside hydrolase family 3 isolated from compost using metagenomic analysis. *J. Biol. Chem.* **2013**, *288*, 14985–14992. [CrossRef]
50. Wu, X.; Zhao, S.; Tian, Z.; Han, C.; Jiang, X.; Wang, L. Dynamics of loops surrounding the active site architecture in GH5_2 subfamily TfCel5A for cellulose degradation. *Biotechnol. Biofuels Bioprod.* **2023**, *16*, 154. [CrossRef]

51. Wu, M.; Bu, L.; Vuong, T.V.; Wilson, D.B.; Crowley, M.F.; Sandgren, M.; Ståhlberg, J.; Beckham, G.T.; Hansson, H. Loop motions important to product expulsion in the Thermobifida fusca glycoside hydrolase family 6 cellobiohydrolase from structural and computational studies. *J. Biol. Chem.* **2013**, *288*, 33107–33117. [CrossRef]
52. Havukainen, R.; Törrönen, A.; Laitinen, T.; Rouvinen, J. Covalent binding of three epoxyalkyl xylosides to the active site of endo-1,4-xylanase II from Trichoderma reesei. *Biochemistry* **1996**, *35*, 9617–9624. [CrossRef]
53. Hsieh, Y.C.; Wu, Y.J.; Chiang, T.Y.; Kuo, C.Y.; Shrestha, K.L.; Chao, C.F.; Huang, Y.C.; Chuankhayan, P.; Wu, W.G.; Li, Y.K.; et al. Crystal structures of Bacillus cereus NCTU2 chitinase complexes with chitooligomers reveal novel substrate binding for catalysis: A chitinase without chitin binding and insertion domains. *J. Biol. Chem.* **2010**, *285*, 31603–31615. [CrossRef] [PubMed]
54. Hidaka, M.; Nishimoto, M.; Kitaoka, M.; Wakagi, T.; Shoun, H.; Fushinobu, S. The crystal structure of galacto-N-biose/lacto-N-biose I phosphorylase: A large deformation of a TIM barrel scaffold. *J. Biol. Chem.* **2009**, *284*, 7273–7283. [CrossRef] [PubMed]
55. Meelua, W.; Thinkumrob, N.; Saparpakorn, P.; Pengthaisong, S.; Hannongbua, S.; Ketudat Cairns, J.R.; Jitonnom, J. Structural basis for inhibition of a GH116 β-glucosidase and its missense mutants by GBA2 inhibitors: Crystallographic and quantum chemical study. *Chem. Biol. Interact.* **2023**, *384*, 110717. [CrossRef] [PubMed]
56. Pengthaisong, S.; Hua, Y.; Ketudat Cairns, J.R. Structural basis for transglycosylation in glycoside hydrolase family GH116 glycosynthases. *Arch. Biochem. Biophys.* **2021**, *706*, 108924. [CrossRef] [PubMed]
57. Pengthaisong, S.; Piniello, B.; Davies, G.J.; Rovira, C.; Ketudat Cairns, J.R. Reaction Mechanism of Glycoside Hydrolase Family 116 Utilizes Perpendicular Protonation. *ACS Catal.* **2023**, *13*, 5850–5863. [CrossRef] [PubMed]
58. Ferrara, M.C.; Cobucci-Ponzano, B.; Carpentieri, A.; Henrissat, B.; Rossi, M.; Amoresano, A.; Moracci, M. The identification and molecular characterization of the first archaeal bifunctional exo-β-glucosidase/N-acetyl-β-glucosaminidase demonstrate that family GH116 is made of three functionally distinct subfamilies. *Biochim. Biophys. Acta* **2014**, *1840*, 367–377. [CrossRef] [PubMed]
59. Shimokawa, M.; Ishiwata, A.; Kashima, T.; Nakashima, C.; Li, J.; Fukushima, R.; Sawai, N.; Nakamori, M.; Tanaka, Y.; Kudo, A.; et al. Identification and characterization of endo-α-, exo-α-, and exo-β-D-arabinofuranosidases degrading lipoarabinomannan and arabinogalactan of mycobacteria. *Nat. Commun.* **2023**, *14*, 5803. [CrossRef]
60. Cobucci-Ponzano, B.; Aurilia, V.; Riccio, G.; Henrissat, B.; Coutinho, P.M.; Strazzulli, A.; Padula, A.; Corsaro, M.M.; Pieretti, G.; Pocsfalvi, G.; et al. A new archaeal beta-glycosidase from Sulfolobus solfataricus: Seeding a novel retaining beta-glycan-specific glycoside hydrolase family along with the human non-lysosomal glucosylceramidase GBA2. *J. Biol. Chem.* **2010**, *285*, 20691–20703. [CrossRef]
61. Huang, M.; Pengthaisong, S.; Charoenwattanasatien, R.; Thinkumrob, N.; Jitonnom, J.; Cairns, J.R.K. Systematic Functional and Computational Analysis of Glucose-Binding Residues in Glycoside Hydrolase Family GH116. *Catalysts* **2022**, *12*, 343. [CrossRef]
62. Sansenya, S.; Mutoh, R.; Charoenwattanasatien, R.; Kurisu, G.; Ketudat Cairns, J.R. Expression and crystallization of a bacterial glycoside hydrolase family 116 β-glucosidase from Thermoanaerobacterium xylanolyticum. *Acta Crystallogr. Sect. F Struct. Biol. Commun.* **2015**, *71*, 41–44. [CrossRef]